Combustion Theory and Modelling, 2014
Vol. 18, No. 3, 454–473, http://dx.doi.org/10.1080/13647830.2014.923116

Triple flame: Inherent asymmetries and pentasectional character

Albert Jordà Juanós* and William A. Sirignano

Department of Mechanical and Aerospace Engineering, University of California, Irvine, CA 92697-3975, USA

(*Received 24 February 2014; final version received 5 May 2014*)

A two-dimensional triple-flame numerical model of a laminar combustion process reflects flame asymmetric structural features that other analytical models do not generate. It reveals the pentasectional character of the triple flame, composed of the central pure diffusion-flame branch and the fuel-rich and fuel-lean branches, each of which is divided into two sections: a near-stoichiometric section and a previously unreported near-flammability-limits section with combined diffusion and premixed character. Results include propagation velocity, fuel and oxidiser mass fractions, temperature and reaction rates. Realistic stoichiometric ratios and reaction orders match experimental planar flame characteristics. Constant density, a one-step reaction, and a mixture fraction gradient at the inlet as the simulation parameter are imposed. The upstream equivalence ratio or the upstream reactant mass fractions are linear or hyperbolic functions of the transverse coordinate. The use here of experimental kinetics data differs from previous analytical works and results in flame asymmetry and different flammability limits. Upstream mixture composition gradient affects propagation velocity, flame curvature, diffusion flame reaction rate, and flammability limits. Flammability limits extend beyond those of a planar flame due to transverse heat and mass diffusion causing the pentasectional character.

Keywords: triple flame; edge flame; diffusion flame; premixed combustion; partially premixed combustion

Nomenclature

A	Pre-exponential factor
c_p	Specific heat under constant pressure
D	Mass diffusivity
E_a	Activation energy
[F], [O]	Fuel and Oxygen molar density
h	Specific enthalpy
L	Domain length
Le	Lewis number
m, n	Reaction orders
P	Pressure
Q	Fuel heat of combustion
R_u	Universal gas constant
t	Time
T	Temperature

*Corresponding author. Email: ajordaju@uci.edu

U	Upstream velocity
U_o	Steady-state upstream velocity
W	Domain width
x, y	Cartesian coordinates
Y_F	Fuel mass fraction
Y_O	Oxygen mass fraction
β_1, β_2	Conserved Shvab–Zel'dovich variables
Δt	Time step
$\Delta x, \Delta y$	Distance between nodes in x and y
ν	Fuel-to-oxygen mass stoichiometric ratio
ρ	Mixture density
Φ	Equivalence ratio
$\dot{\omega}$	Fuel reaction rate

1. Introduction

Triple flames have been described as tri-brachial structures consisting of a fuel-rich premixed flame, a fuel-lean premixed flame and a diffusion flame [1,2]. The two premixed flames form a curved flame front followed by a trailing edge that constitutes the body of the diffusion flame. The diffusion flame starts at the point where the two premixed flames meet, where the inflowing mixture is at stoichiometric proportions. Such flames, also called edge flames, appear in flows characterised by gradients of concentrations of the reactants and they have been studied during the past decades (see Section 2).

Many combustion processes rely on the burning of gaseous reactants that initially flow separately and subsequently form a mixing layer, generally with mixing beginning upon their entering the combustion chamber. They react within thin reaction zones under space- and time-varying reactant concentration conditions. Such reaction zones are located at the stoichiometric surfaces and form a diffusion flame. In non-premixed turbulent conditions, such diffusion flames could be stretched and quenched locally due to velocity fluctuations, when the heat diffusing away from the reaction zone is not balanced by the heat produced by combustion. The characteristic flame structure that is observed at an edge of the stoichiometric surface bordering the extinction zone can be modelled locally by a triple flame [3].

Thus, triple flames are physically embodied in real combustors, and it is important to avoid undesirable combustion conditions there such as flame flashback or blow-off. Therefore, it is desirable to understand the propagation characteristics of these flames and how to stabilise them. Furthermore, the speed of propagation of the triple flame determines such important properties as the flame surface increase rate in non-premixed combustion and the lift-off distance in lifted flames at burners [3].

The goal of the present numerical study is to analyse triple flames with a simplified model that describes qualitatively how the premixed branches can be split into two sections, which display the pentasectional character of the triple flame (see Figure 1). This discussion will focus on multidimensional, steady flames where all five sections appear simultaneously. Only monotonic variation of concentration in space will be considered. The modelling performed in the present work also addresses issues such as flame stabilisation, flammability limits, temperature and shape. The background for this study will be explained in the following literature review section.

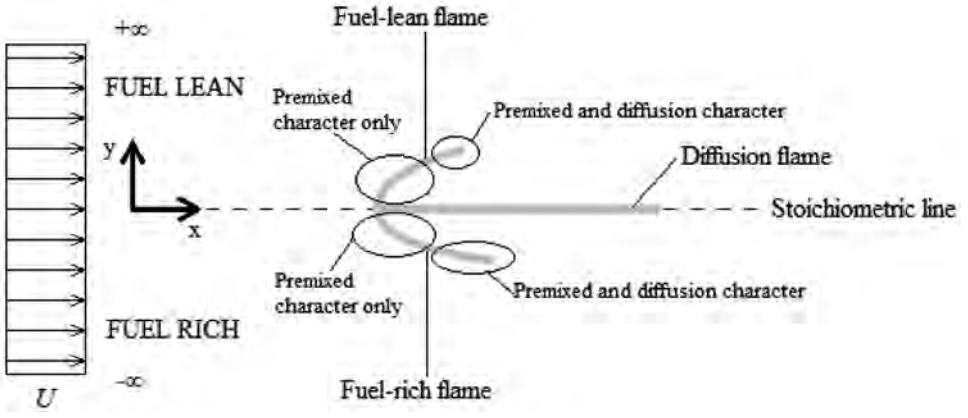

Figure 1. Pentasectional triple flame sketch and problem domain.

2. Literature review

Triple flames have been investigated experimentally, analytically and numerically. They were first observed in a buoyant methane layer experiment [4]. Other experimental studies in which triple flames appeared include [5–12]. These studies helped to understand triple flame properties such as propagation, stabilisation, liftoff and blowout behaviour, and concentration and dilution effects. Collectively, they cover several flow configurations, including non-premixed jets, laminar mixing layers, two-dimensional and axisymmetric counterflows, and liquid-film fuel combustors.

To the best knowledge of the authors, triple flames were first analysed for an unsteady premixed flame moving through a stratified combustible mixture forming a diffusion flame as the premixed flame passed from a fuel-rich zone to a fuel-lean zone [13]. Triple flames were also identified as transient laminar flamelets in the combustion of turbulent diffusion flames [14,15]. The analytical formulation was developed accounting for approximations such as small upstream concentration gradients (also called slowly-varying triple flames) [1,2], or parabolic flame paths [3]. These studies helped gain insight to Lewis number effects on flame structure and propagation speed decrements resulting from increments in the upstream mixture ratio. They also revealed that the adiabatic planar flame speed is an upper boundary for the propagation speed of triple flames for the constant-density case. Another simple analytical method was used to study buoyancy effects on triple flames [16].

The articles that used numerical approaches to triple flames may be classified depending on three important aspects: the use of constant or variable density, prescribed unity or non-unity Lewis number for the species, and one-step versus detailed chemical kinetics. Table 1 shows a chronologically ordered list of articles that presented numerical results on triple flames.

In solving problems that involve reacting flows, the choice of the model for the chemical kinetics is significant. In 1981, Westbrook and Dryer [27] examined simplified reaction mechanisms for the oxidation of hydrocarbon fuels using a numerical laminar flame model entailing one and two global reaction steps and quasi-global mechanisms. The reaction-rate parameters were changed for different combinations of hydrocarbon fuels and air, and such parameters were adjusted to provide the best agreement between computed and experimentally observed planar flame speeds. The theoretical models that use 1-step chemical reaction mechanisms entailing parameters obtained from experimental analysis have been

Table 1. Chronological classification of numerical studies.

Reference no.	Density	Lewis no.	Chemical kinetics	Laminar/Turbulent
[1]	Constant	Unity	1-step, unmatched parameters	Laminar
[17]	Constant	Unity	1-step, unmatched parameters	Laminar
[6]	Constant	Unity	1-step, unmatched parameters	Laminar
[18]	Variable	Non-unity	1-step, unmatched parameters	Laminar
[19]	Variable	Unity	1-step, unmatched parameters	DNS
[20]	Constant	Unity	1-step, unmatched parameters	Laminar
[21]	Constant	Variable	1-step, unmatched parameters	Laminar
[9]	Variable	Non-unity	10-step, detailed kinetics	Laminar
[22]	Variable	Non-unity	C_1, detailed kinetics	DNS
[23]	Variable	Non-unity	38-step, detailed kinetics	DNS
[16]	Variable	Unity	1-step, unmatched parameters	Laminar
[24]	Variable	Non-unity	38-step, detailed kinetics	DNS
[25]	Variable	Non-unity	1-step, matched parameters	Laminar
[26]	Variable	Unity	1-step, matched parameters	DNS

identified in Table 1 as 'matched'. Chemical kinetics models that are arbitrary in that sense have been labelled 'unmatched'.

Note that all the numerical studies listed in Table 1 that use one-step reaction mechanisms assume chemical kinetics with unity reaction order and identical molecular weights for each reactant except [25], in which the activation energy was artificially adapted as a function of fuel-to-oxygen equivalence ratio to match real kinetic rates. A study of triple flames entailing a one-step reaction mechanism equipped with the experimentally obtained parameters from [27] is missing. Thus, this paper will address that need. We will assume simplifications such as constant density and unit Lewis number, but the chemical reaction term in the equations will be equipped with the kinetics parameters provided by [27] and the reactants will be balanced in proper mass proportions. We will no longer maintain the artificial symmetry of many previous research works with regard to the concentration and molecular weight of each reactant.

Although the constant-density assumption is often designated as low heat release, it does not mean, for example, that the amount of heat produced by the combustion process is low compared with the enthalpy of the unburned gas. The commonly used description 'low heat release' is poor because the energy per unit mass of the combustible mixture is actually not reduced. Rather, the resulting gas expansion is ignored; so, 'constant density' is a superior description. As opposed to the low-heat release cases in which the triple flame propagation velocity is bounded above by the planar premixed flame speed, heat release causes gas expansion and redirection of the flow that produces triple flame propagation velocities greater than the planar flame velocity. These effects depend also on the mixture ratio gradient at the inlet. The heat release causes an expansion in the gas field which results in the slowing of the incoming unburned gases as they approach the flame front [18]. Consequently, the free stream velocity exceeds the local flame velocity. Aside from the effects that heat release has on flame propagation, using unity reaction orders and unmatched chemistry parameters results in flame front shape profiles that show symmetric properties with respect to the stoichiometric line. Symmetry will be prevented by the kinetics that we will use in the present study.

A review of edge-flames described tribrachial flames as ignition fronts with positive speeds characterised by a trailing diffusion flame [28]. The solutions showed structures

which, after initial transients, propagated at well defined speeds and had unchanging shape. Under the mentioned assumptions, the present work reports results that are in agreement with these features. However, some new features related to the pentasectional character will be identified and discussed. The new model, numerical details and results are presented in the following sections.

3. Model and analysis

3.1. *Formulation of differential equations*

The two-dimensional transient model presented is subject to the following assumptions: fluid consisting of a mixture of fuel and oxidiser (i.e. propane and air); laminar flow; uniform velocity field with x-velocity component only (U); unit Lewis number ($Le = 1$); constant thermal conductivity and specific heat; neglected radiative transfer; and constant density. The thermal conductivity and the specific heat will be evaluated for the calculation of thermal diffusivity at a mean flame temperature while the density will be assessed at the upstream conditions. The value of the heat of combustion Q is taken from the literature [29]. The lower heating value is assumed throughout this study, which implies that none of the water in the products condenses. The upstream velocity U will be adjusted conveniently in order to stabilise the flame. Changes in U imply a change in the pressure gradient. However, the pressure time derivative term is approximated to be zero in the energy equation because the time change in pressure due to these small velocity adjustments will be very small compared to the changes in temperature through the domain. Furthermore, we are interested in the steady-state solution reached asymptotically in time, and temporal changes during the transient part of the simulation are less interesting.

We define the following two Shvab-Zel'dovich variables, as well as the differential operator $\mathscr{L}$:

$$\beta_1 = Y_\mathrm{F} - \nu Y_\mathrm{O}, \quad \beta_2 = h + \nu Y_\mathrm{O} Q = c_p T + \nu Y_\mathrm{O} Q \tag{1}$$

$$\mathscr{L}(u) = \frac{\partial u}{\partial t} + U\frac{\partial u}{\partial x} - D\nabla^2 u. \tag{2}$$

Under the proposed hypothesis, selected combinations of the equations of energy, fuel and oxygen species yield

$$\mathscr{L}(\beta_1) = 0, \quad \mathscr{L}(\beta_2) = 0, \quad \mathscr{L}(Y_\mathrm{F}) = -\frac{\dot{\omega}}{\rho}(\beta_1, \beta_2, Y_\mathrm{F}). \tag{3}$$

We will consider the flame to be propagating in the negative x-direction in the laboratory through a quiescent combustible mixture. We seek the final steady velocity of propagation $U_o > 0$. If the reference frame moves with the flame, we have a steady free stream at velocity U_o flowing in the positive x-direction. Then, $U = U_o$ and the time derivative in operator $\mathscr{L}$ becomes zero. However, we do not know U_o *a priori*, which is an eigenvalue of the problem.

In general, we must solve the system of equations (3). However, if we restrict the fuel and oxidiser mass fractions at the inlet to be linear functions of y, we can show that then only a single equation has to be solved.

3.2. *Initial and boundary conditions*

Instead of setting initial conditions for β_1 and β_2, it is more intuitive to set them for the fuel and oxygen mass fractions and for the temperature. Hyperbolic tangent functions of x are used to represent the decreases in fuel and oxygen mass fractions or temperature rise across the flame. The initial conditions for β_1 and β_2 are obtained using the three previous initial conditions in Equations (1). The initial velocity value is taken from experimental data for premixed stoichiometric planar flames.

The boundary conditions are imposed on the distributions of fuel, oxygen and temperature, and they prescribe the following boundary conditions for the functions β_1 and β_2.

At $x = L$:

$$\frac{\partial Y_{\mathrm{F}}}{\partial x} = 0, \quad \frac{\partial Y_{\mathrm{O}}}{\partial x} = 0, \quad \frac{\partial T}{\partial x} = 0. \tag{4}$$

At $y = \pm W/2$:

$$\frac{\partial^2 Y_{\mathrm{F}}}{\partial y^2} = 0, \quad \frac{\partial^2 Y_{\mathrm{O}}}{\partial y^2} = 0, \quad \frac{\partial^2 T}{\partial y^2} = 0. \tag{5}$$

For $x = 0$ (inlet), the mixture ratio is a prescribed function of y and its gradient is varied and used as a parameter of the problem. In these conditions, one side of the domain becomes fuel-rich whereas the other side becomes fuel-lean. Four types of transverse variations for upstream flow are considered: linear variation of mass fraction; hyperbolic tangent variation of mass fraction; linear variation of equivalence ratio; and hyperbolic tangent variation of equivalence ratio.

The linear variation of mass fraction allows an analytical simplification. The hyperbolic tangent variation of mass fraction presents a flow similar to a mixing layer. The hyperbolic tangent variation of equivalence ratio resembles profiles used previously [18]. The linear variation of equivalence ratio provides an interesting comparison. The use of equivalence ratio is especially useful in studying flammability limits.

3.2.1. *Linear mass-fraction profile*

Let us now consider the particular case in which the mass fractions are linear in y far upstream ($x \to -\infty$). We also prescribe the temperature (or enthalpy) at the inlet.

$$Y_{\mathrm{F}_{-\infty}} = Y_{\mathrm{F}_o} + k_1 y, \quad Y_{\mathrm{O}_{-\infty}} = Y_{\mathrm{O}_o} + k_2 y, \quad h_{-\infty} = h_o, \quad T_{-\infty} = T_o. \tag{6}$$

Y_{F_o} and Y_{O_o} are in stoichiometric proportions. A fuel-rich mixture exists for $y < 0$ and a fuel-lean mixture occurs for $y > 0$. Then, $k_1 < 0 < k_2$.

Let us define

$$a = \nu k_2 - k_1 > 0, \quad H = h_o + \nu Y_{\mathrm{O}_o} Q, \quad b = \nu k_2 Q > 0. \tag{7}$$

Then

$$\beta_{1_{-\infty}} = -ay, \quad \beta_{2_{-\infty}} = h_o + \nu Y_{\mathrm{O}_o} Q + \nu k_2 Q y = H + by. \tag{8}$$

Note that $\beta_1 = -ay$ and $\beta_2 = H + by$ become zero when differentiated once by t or x or twice by y. Therefore, they satisfy $\mathscr{L}(\beta) = 0$ as well as satisfying the upstream and side boundary conditions. We have solutions to the first two equations in (3), which may be substituted into the third one so that

$$\mathscr{L}(Y_{\mathrm{F}}) = -\frac{\dot{\omega}}{\rho}(-ay,\, H + by,\, Y_{\mathrm{F}})\,. \tag{9}$$

Thus, we have shown that when the mass fractions of the reactants at the inlet are linear functions, only Equation (9) must be solved for Y_{F}. Since β_1 and β_2 are known, back substitution into Equations (1) will provide Y_{O} and T (which is related to the enthalpy). The linear profiles upstream of the flame front imply that diffusion in the y-direction is uniform and the composition will not vary along any streamline before it reaches the flame.

3.2.2. *Hyperbolic tangent mass-fraction profile*

In reality, it would be difficult to find purely linear functions of y at the inlet of a combustor. In the modelling of mixing layers, hyperbolic tangent functions are usually used to represent the velocity profile across the layer (see for example [30,31]). The hyperbolic tangent functions for the reactants mass fractions at the inlet are given by Equations (10):

$$Y_{\mathrm{F}_{-\infty}} = Y_{\mathrm{F}_o}\,[1 + \tanh(k_3 y)]\,, \qquad Y_{\mathrm{O}_{-\infty}} = Y_{\mathrm{O}_o}\,[1 + \tanh(k_4 y)]\,. \tag{10}$$

To be consistent with the criteria used before, we choose to have a fuel-lean mixture for $y > 0$ and a fuel-rich mixture for $y < 0$. Then $k_3 < 0$ and $k_4 > 0$. In order to make this hyperbolic case comparable to the linear case, the parameters k_3 and k_4 are related to the linear slopes k_1 and k_2 so that the maximum gradients of the hyperbolic tangent profiles match the slopes of the linear profiles. For any case entailing nonlinear functions at the inlet, the problem cannot be reduced to solving a single equation. Instead, the system of equations (3) has to be solved. With this profile, diffusion fluxes in the y-direction upstream of the flame are not uniform with y. Accordingly, some change of composition for a given streamline will occur upstream of the flame.

3.2.3. *Linear equivalence ratio profile*

For the cases in which the inflowing equivalence ratio is prescribed as a linear function we use

$$\Phi_{-\infty} = k_5 y + k_6. \tag{11}$$

3.2.4. *Hyperbolic tangent equivalence ratio profile*

For the cases in which the inflowing equivalence ratio is prescribed as a hyperbolic tangent function we use

$$\Phi_{-\infty} = 0.5[1 + \tanh(k_7 y)]. \tag{12}$$

3.3. *Chemical kinetics*

Let us consider the Arrhenius one-step form for the reaction rate, where [F] and [O] are the molar density for fuel and oxygen species, respectively, and $T - T_o$ is used to confront the 'cold-boundary difficulty' [32]:

$$\frac{d[\mathrm{F}]}{dt} = [\mathrm{F}]^m[\mathrm{O}]^n A \ \exp\left\{-\frac{E_a}{R_u\,(T - T_o)}\right\}, \quad \dot{\omega} = \rho\frac{dY_\mathrm{F}}{dt}. \tag{13}$$

For comparison purposes, two different sets of the kinetics parameters will be used:

- matched kinetics with constants from [27] (propane and air): $m = 0.1$, $n = 1.65$, $E_a/R_u = 15{,}098$ K, $A = 4.84 \times 10^9\,(\mathrm{kmol\ m^{-3}})^{-0.75}\,\mathrm{s^{-1}}$, $T_0 = 300$ K;
- unmatched kinetics: $m = 1$, $n = 1$.

Previous studies that used unmatched kinetics tended to provide qualitative explanations of the flame shape and propagation rather than quantitative descriptions. Our goal here is to compare the qualitative differences between the use of matched and unmatched kinetics. To achieve this, the reaction orders are switched to unity. The original values of the oxygen molecular weight, activation energy E_a and pre-exponential factor A are kept the same. However, the heat of combustion Q is reduced (by a factor of six) so that the propagation velocity for stoichiometric conditions in the unmatched kinetics case equals the velocity calculated later with the original kinetics for propane and air ($0.37\ \mathrm{m\ s^{-1}}$). The numerical scheme specifications will be presented in the following section.

3.4. *Numerical method and convergence*

The domain is discretised using a Cartesian uniformly spaced two-dimensional mesh. An explicit forward difference is used for the transient terms, in which Δt represents the step in time, and a central difference is used for the diffusion terms. The time step is chosen so that it satisfies the numerical stability requirements; we also use an upwind scheme for the advection term.

After starting the code, the shape of the fuel mass fraction profile changes every step in time, from its initial profile towards a steady shape governed by Equation (3). Taking this into account, the upstream velocity is not changed during this initial period of simulation. Afterwards, the 'cliff' of the fuel mass fraction moves forward or backward depending on how different the upstream velocity U is compared to U_o. We adjust this velocity until the 'cliff' does not move. To achieve this goal, we focus on the peak value of the reaction rate and observe its change in position over time $x_{\max}(t)$, as shown in Figure 2. In the general case, the reaction rate will be a function of x and y. We will focus on the y-coordinate in which the peak of the reaction rate is found.

The upstream velocity is adjusted according to the following increment:

$$\Delta U = \frac{x_{\max}(t + \Delta t) - x_{\max}(t)}{\Delta t}. \tag{14}$$

Note that ΔU is positive when the flame moves forward. Therefore, the adjusted upstream velocity is given by

$$U^{\mathrm{new}} = U^{\mathrm{old}} - \Delta U. \tag{15}$$

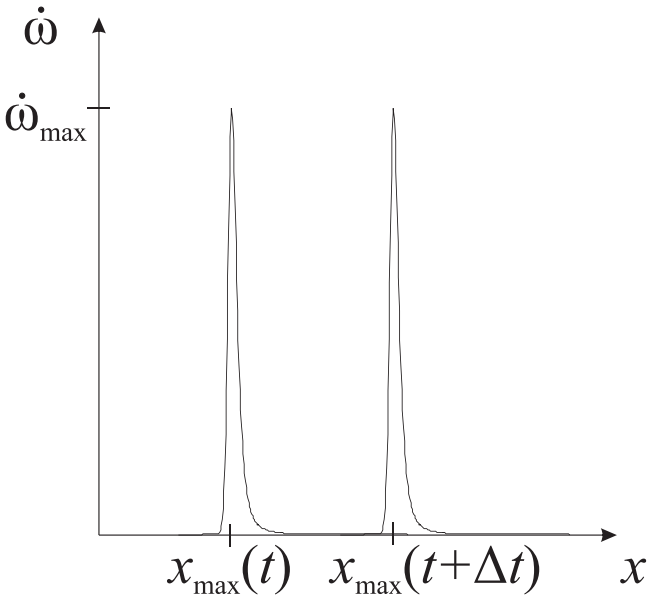

Figure 2. Position change of the reaction-rate peak.

After some time of repeating this iterative process during the simulation, the upstream velocity increment goes to 0 ($\Delta U \rightarrow 0$) and the upstream velocity becomes U_o. The criterion to end the simulation is the condition that ΔU is zero for a sufficiently long period of time (i.e. $10^3 \times \Delta t$).

The mesh has been refined until the results have become mesh-independent, resulting in 500 nodes in each direction for a domain that is 5 mm long and 5 mm wide. When considering the minimum number of nodes to be used, we must also bear in mind that the most drastic gradients in the physical variables occur within the reaction zone. To capture these gradients successfully with the reaction zone thickness about one-half of a millimeter, 500 nodes are used in the *x*-direction, yielding about 50 nodes in the reaction zone. Farther downstream, there are about 25 nodes across the diffusion flame in the *y*-direction. These quantities are deemed to be sufficient.

In order to show that the results are independent of the size of the domain, calculations have been performed for different domain sizes while keeping the same Δx and Δy as for the 5 mm case. The results show their independence of the domain size.

4. Results and discussion

4.1. *Flammability limits: Pentasectional character*

One of the goals of this section is to compare the differences in flammability limits between our model and the one used by Westbrook and Dryer [27] for planar flames. They reported equivalence ratio values for the fuel-lean and fuel-rich flammability limits of a one-dimensional planar flame of 0.5 and 3.2, respectively (for propane and air). Reduction of our model to the one-dimensional case yields 0.5 and 2.8 for these two limits. So, good agreement is found for the planar case which corresponds to the experimental values. However, the theory now predicts different values for the two-dimensional case, a finding

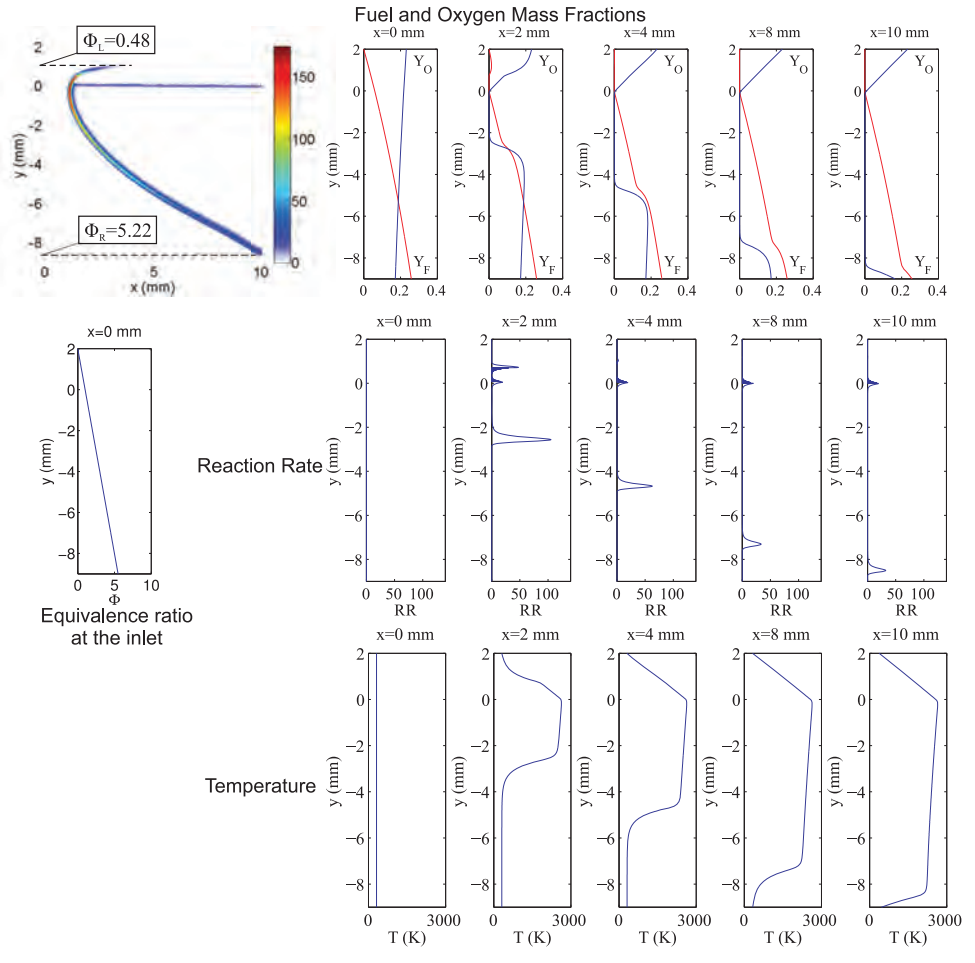

Figure 3. Scalar variables – linear equivalence ratio at the inlet (maximum equivalence ratio = 5.5).

that has not previously been reported. Results for the two-dimensional problem are shown in Figures 3, 4 and 5. The plots portray the reaction rate as well as the scalar quantities (reactants mass fractions, reaction rate and temperature) at several *x*-stations when the equivalence ratio at the inlet varies linearly from 0 at the fuel-lean side to different finite values at the fuel-rich side.

The fuel-lean equivalence ratio limits for these three cases are very close to the value reported [27]. According to the 3.2 fuel-rich limit for a planar flame, which slightly exceeds the experimental value, we might expect to see the fuel-rich premixed flame disappearing in Figures 3–5, but instead it extends beyond the boundary of the computational domain. To address this issue, we analyse two more cases with hyperbolic tangent functions for the equivalence ratio at the inlet: one varying from 0 to 10 and the other one varying from pure fuel to pure air. See Figures 6 and 7, respectively.

As seen in Figure 6, the fuel-lean flammability limit has been extended with respect to the 0.5 encountered in the previous cases. The fuel-rich flame is still extending beyond the computational boundary. In Figure 7, we see a fuel-lean limit which is even leaner

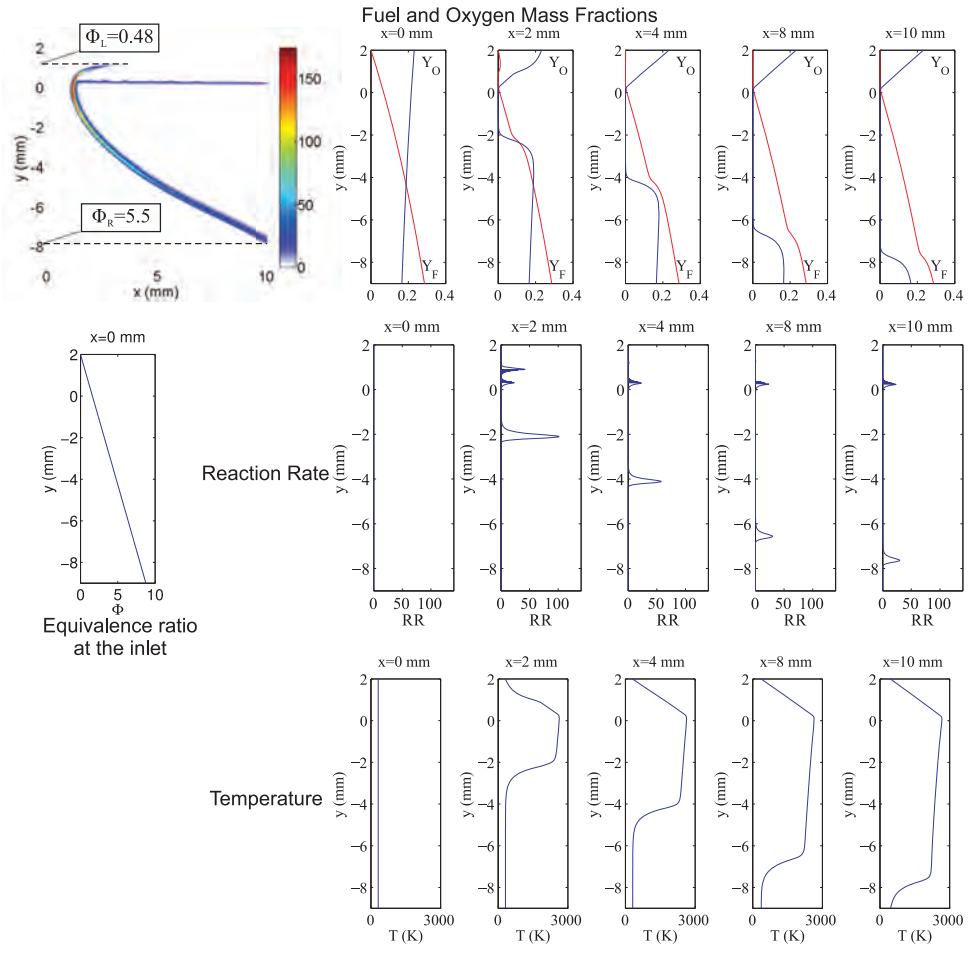

Figure 4. Scalar variables – linear equivalence ratio at the inlet (maximum equivalence ratio = 6.3).

than in the previous figures and the planar flame. As greater gradients are imposed, greater temperature and mass fraction gradients in the *y*-direction appear with greater heat and mass transfer in the *y*-direction, which aids the extension of the fuel-lean flammability limit. On the other hand, the fuel-rich flame comes to an end at an equivalence ratio of 6.53. The reason for this differences in the fuel-rich flammability limit is the presence of oxygen. The last case goes to pure fuel at the computational boundary, meaning that the amount of oxygen is almost zero for a substantial distance from the negative *y* boundary. Still, in these cases, the amount of oxygen present on the fuel-rich side is still large enough to support the combustion.

These results suggest a study of the transverse heat and mass transfer, especially near the flammability limits. For the fuel-lean flame in Figures 3–7, fuel and oxygen are diffused towards the lean flame in the negative *y*-direction from outside the flame region. Heat is diffused in the positive *y*-direction towards the lean flame from inside the flame region. For the fuel-rich flame in Figures 6 and 7, fuel and oxygen are diffused towards the rich flame in the positive *y*-direction from outside the flame region. Heat is diffused in the negative *y*-direction towards the rich flame from inside the flame region. The fluxes of fuel mass

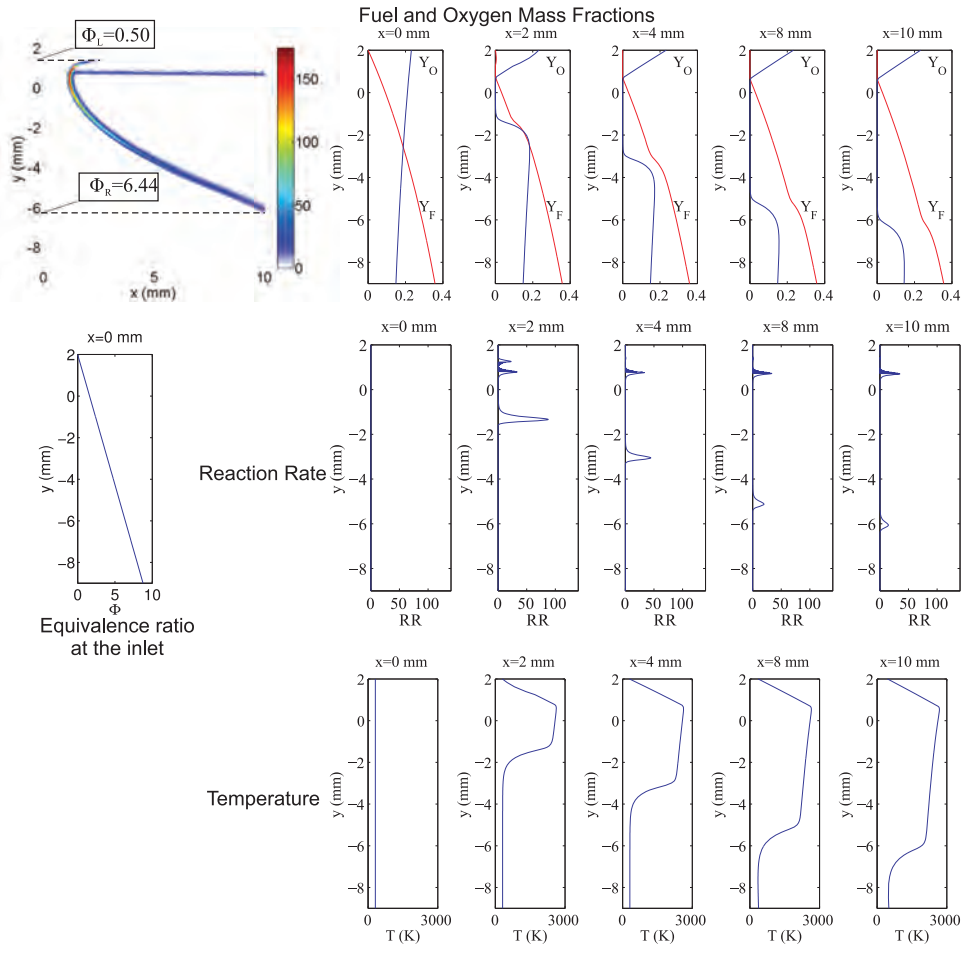

Figure 5. Scalar variables – linear equivalence ratio at the inlet (maximum equivalence ratio = 8.75).

fraction in the x- and y-directions, F_x and F_y respectively, are defined in Equations (16):

$$F_x = \left| UY_{\mathrm{F}} - D\frac{\partial Y_{\mathrm{F}}}{\partial x} \right|, \quad F_y = \left| D\frac{\partial Y_{\mathrm{F}}}{\partial y} \right|. \tag{16}$$

The fluxes of the oxygen mass fraction are calculated in the same fashion by replacing by oxygen in Equations (16). Table 2 shows computations of such fluxes for Figures 6 and 7 at several x-positions. Calculations are made at the flame front. The evolution in x of the ratio between the fluxes in the x-direction to the y-direction shows that the premixed branches tend to develop some diffusion character with increasing downstream distance. Although the hyperbolic tangent profile has F_y decreasing with increasing y magnitude, the ratio F_x/F_y at the flame front is generally decreasing which implies an increasing dependence on transverse diffusion as the flammability limits are approached. This diffusion allows extension of the limits. This character is identified here as the pentasectional character of the triple flame. Essentially, each 'premixed' branch of the flame can be divided into two

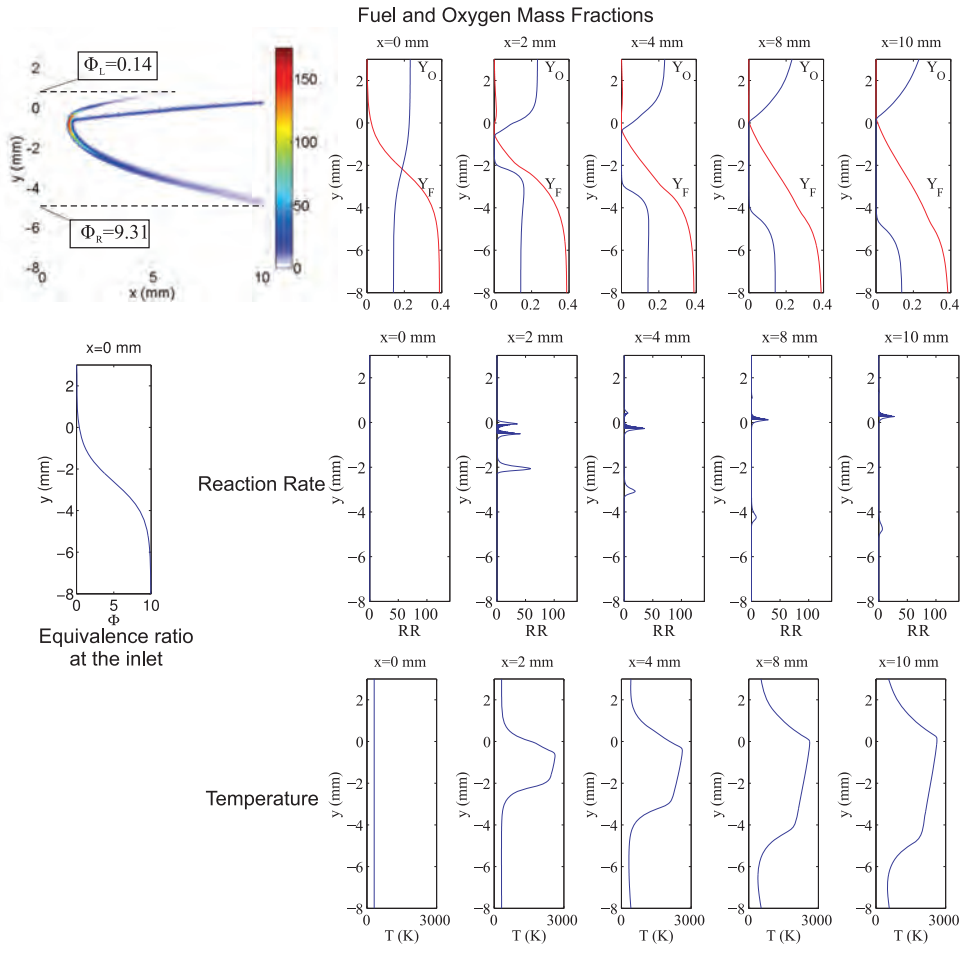

Figure 6. Scalar variables – hyperbolic tangent mass fractions at the inlet (maximum equivalence ratio = 10).

sections: one section near stoichiometric conditions which is predominantly premixed and a section near the flammability limits where a combined diffusion and premixed character exists. Computations of the same fluxes at the trailing diffusion flame show clear dominance of diffusion transport in the *y*-direction, as expected because it is a pure diffusion flame.

4.2. *Flame structure and propagation*

A qualitative analysis of the flame propagation features and shape is presented in this section.

Figure 8 shows the flame propagation velocity versus upstream mixture gradient for both the linear and hyperbolic tangent functions for the reactant mass fractions at the inlet. The slope percentage shown in the abscissa axis is based on the maximum linear slope of the upstream fuel mass fraction. The dashed lines are least square fits to the numerical data. It can be seen how the triple-flame propagation velocity decreases as the mixture gradient is increased. The flame with hyperbolic functions at the inlet is found to

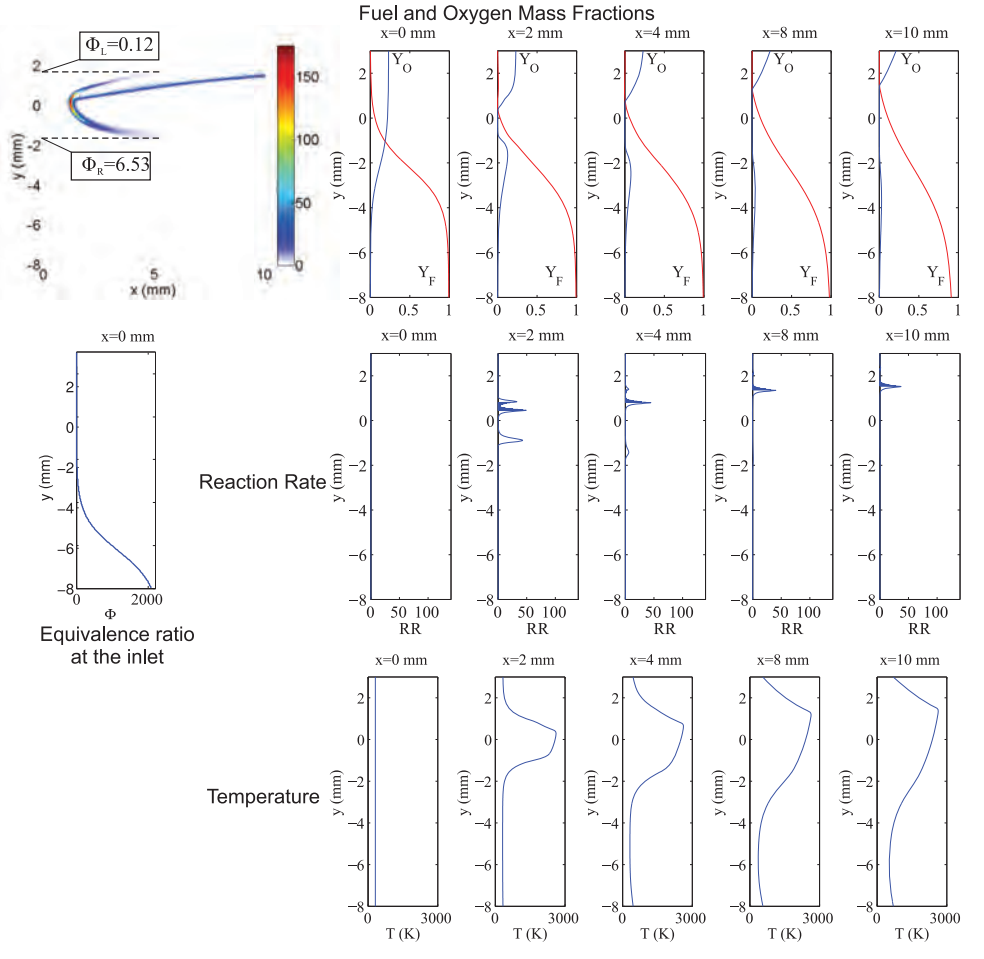

Figure 7. Scalar variables – hyperbolic tangent mass fractions at the inlet (pure fuel and pure air at the boundaries).

propagate slightly more slowly than for the linear case. The solid line corresponds to the stoichiometric planar flame propagation velocity and it is an upper limit of the triple flame propagation velocity. As expected, this result is in qualitative agreement with [1] which neglected density variation, an assumption that is also made in this study. The analysis with linear mass fraction variations at the inlet is repeated with the use of unmatched kinetics

Table 2. Oxygen mass fraction fluxes towards the fuel-rich flame branch and fuel mass fraction fluxes towards the fuel-lean flame branch.

		$x = 2$ mm			$x = 4$ mm			$x = 8$ mm		
		F_x	F_y	F_x/F_y	F_x	F_y	F_x/F_y	F_x	F_y	F_x/F_y
Oxygen	Figure 6	0.04	0.014	2.86	0.025	0.011	2.27	0.02	0.0091	2.20
	Figure 7	0.033	0.013	2.54	0.0121	0.006	2.02	0.0093	0.0031	3.00
Fuel	Figure 6	0.0027	0.002	1.35	3.65e−4	5.3e−4	0.69	1e−4	2e−4	0.50
	Figure 7	0.0024	0.0018	1.33	3.5e−4	4.5e−4	0.78	1.2e−4	1.6e−4	0.75

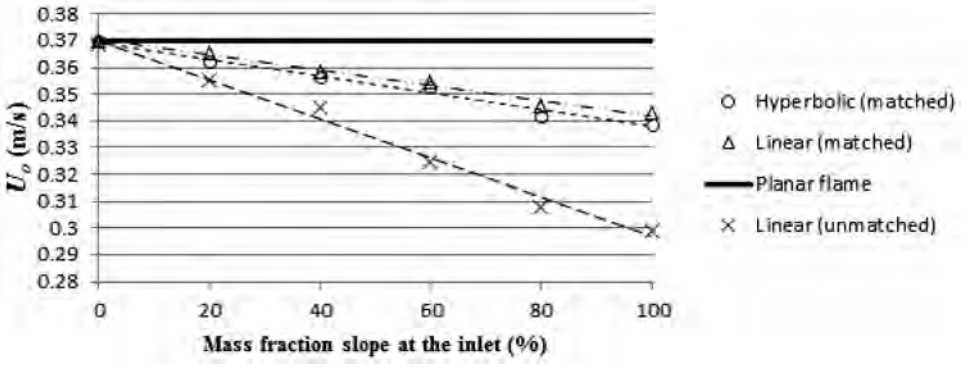

Figure 8. Triple flame propagation velocity versus mass fraction slope at the inlet.

to assess the qualitative effects on the flame features. The propagation velocity for the unmatched kinetics is lower than for the original kinetics and is also bounded above by the planar flame velocity.

The upstream mixture ratio gradient variations also affect the flame structure. As the gradient is increased from Figure 3 to Figure 7, the flame curvature becomes more pronounced, especially on the fuel-lean side, and a greater amount of reactants is left unburned behind the flame. The diffusion transport in the transverse flow direction brings these species to the stoichiometric line in which the diffusion flame burns them. With increasing inlet gradient, this transport of species is greater too, which in turn makes the diffusion flame stronger. The temperature profile behind the flame is a maximum around the stoichiometric line ($y = 0$) and then it decreases to the sides. This decrement is more substantial on the fuel-lean side, which has a more curved flame front. So, the temperature on the fuel-lean side is not as high as on the fuel-rich side. Thus, an asymmetric behaviour of the physical properties can be noticed, even for small gradients. This is in contrast to the results provided by other studies (see Section 2), which use unmatched chemical kinetics and obtain symmetric results. Figures 9 and 10 show the reaction-rate profiles

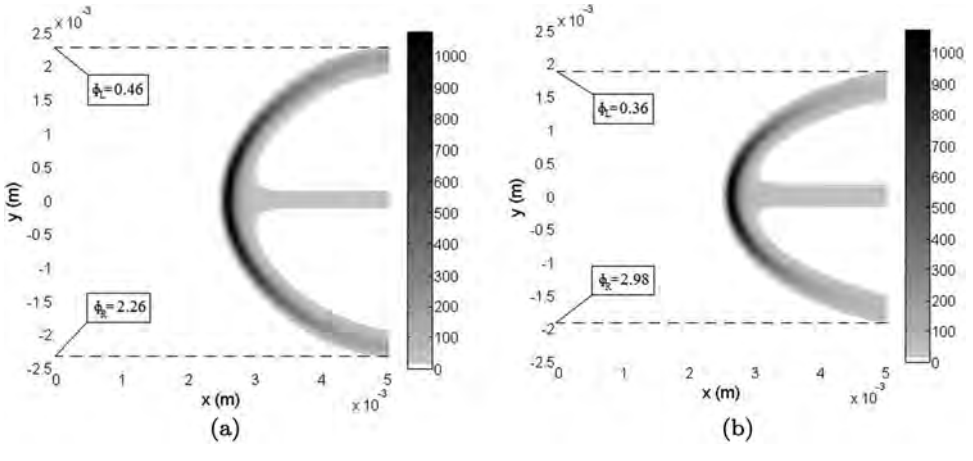

Figure 9. Reaction rates (unmatched kinetics, upstream linear mass fractions). (a) Slope at the inlet = 40%; (b) slope at the inlet = 60%.

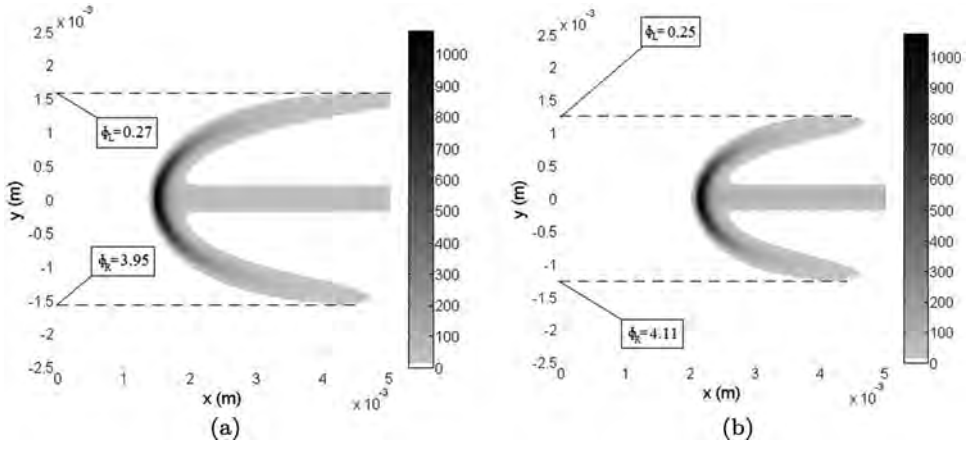

Figure 10. Reaction rates (unmatched kinetics, upstream linear mass fractions). (a) Slope at the inlet = 80%; (b) slope at the inlet = 100%.

using our model with unmatched kinetics. Indeed, symmetric distributions with respect to the stoichiometric line are obtained for all the physical quantities. For this case, increasing the inlet gradient also makes the diffusion flame stronger, and the flame curvature becomes more pronounced. The effect on the flammability limit extension as the inlet gradient is increased is maintained with the unmatched kinetics. Table 3 shows the fluxes F_x and F_y for Figures 9(b) and 10. As for the matched kinetics case, now the ratio F_x/F_y also decreases at the flame front with increasing y. Hence, the triple flame also develops a pentasectional character, which is emphasised for greater gradients at the inlet.

To gain more insight on the flame shape, we analyse two characteristic zones of the triple flame, which are the most forward point and the maximum reaction-rate point. Figure 11 shows a three-dimensional plot of the reaction rate. The diffusion flame can be seen at $y = 0$, and the curved flame front has the maximum reaction rate near the stoichiometric line. In Figure 11, the most forward point corresponds to the minimum x-location at which the reaction rate is different from zero. This is the leading point of the triple flame. The maximum reaction-rate point has an associated upstream mixture ratio that should correspond to the mixture ratio that yields the maximum reaction rate for the

Table 3. Unmatched kinetics: oxygen mass fraction fluxes towards the fuel-rich flame branch and fuel mass fraction fluxes towards the fuel-lean flame branch.

		Distance from the flame leading edge								
		0.5 mm			1.5 mm			2.5 mm		
		F_x	F_y	F_x/F_y	F_x	F_y	F_x/F_y	F_x	F_y	F_x/F_y
Oxygen	60%	0.0907	0.0289	3.1391	0.0469	0.0195	2.3852	0.0210	0.0141	1.4927
	80%	0.0776	0.0219	3.5425	0.0331	0.0147	2.2486	0.0144	0.0086	1.6642
	100%	0.0648	0.0185	3.5029	0.0203	0.0109	1.8709	0.004	0.0037	1.0808
Fuel	60%	0.0913	0.0316	2.8933	0.0486	0.0210	2.3126	0.0238	0.0170	1.4002
	80%	0.0696	0.0344	2.0241	0.0329	0.0159	2.0686	0.0140	0.0094	1.4873
	100%	0.0601	0.0282	2.1275	0.0174	0.0118	1.47	0.0041	0.0038	1.077

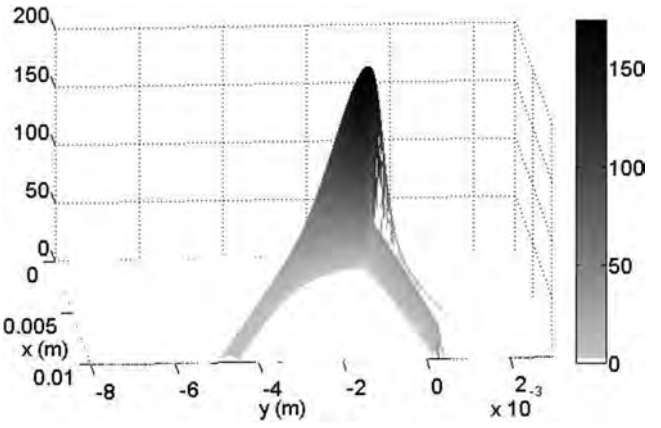

Figure 11. Reaction rate 3D plot (corresponds to Figure 6).

one-dimensional case. Reduction of our model to this case shows that the flame propagation velocity and maximum reaction rate peak slightly off stoichiometric conditions, to the fuel-lean side, while the temperature peaks at stoichiometric conditions. A comparison is made with the information found for the one-dimensional analysis. The location of the most forward point is also compared with the location of the maximum reaction-rate point.

As shown in Figure 12(a), for the case with linear mass fractions at the inlet and matched kinetics, the peak of the reaction rate is located at the fuel-lean side, and it moves towards the stoichiometric line as we increase the slope. This agrees with the one-dimensional result. The most forward point on the flame front is located on the fuel-rich side and it also moves towards the stoichiometric line as we increase the slope. Using unmatched kinetics, both points appear on the stoichiometric line regardless of the upstream mixture gradient.

For the case with hyperbolic tangent mass fractions at the inlet (Figure 12(b)), the peak of the reaction rate is located at the fuel-lean side ($y > 0$), and it moves towards the stoichiometric line as we increase the mixture gradient. This result is in agreement with the one-dimensional result and the two-dimensional linear case. The most forward point is located on the fuel-rich side and it also moves towards the stoichiometric line as the upstream mixture gradient is increased. This behaviour is in agreement with the two-dimensional linear case.

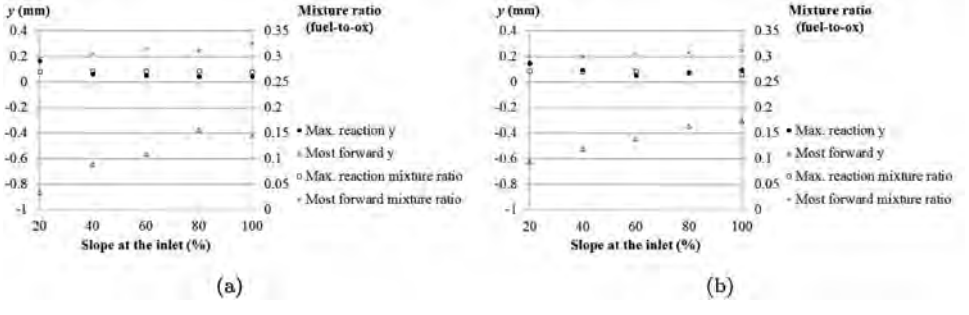

Figure 12. Location of the maximum reaction rate and most forward points. (a) Linear mass fractions at the inlet; (b) hyperbolic tangent mass fractions at the inlet.

5. Conclusions

A numerical two-dimensional analysis has been presented to model triple flames. The results reflect that imposition of greater transverse mixture ratios extend the flammability limits beyond those corresponding to a planar flame. This result is due to an increased transport of heat and mass in the transverse direction of the flow. Studying the mass fluxes of the reactants towards the lateral 'premixed' flame branches shows that they evolve from premixed flames at near stoichiometric conditions to a combination of premixed and diffusion flames near the flammability limits. So, each 'premixed' branch can be separated into two sections, which is identified as the pentasectional character of the triple flame.

Linear and hyperbolic tangent functions of the transverse coordinate have been used to prescribe the equivalence ratio or the reactants mass fractions at the inlet. Linear and hyperbolic tangent variations of inflowing mass fractions produce qualitatively similar results. The flame propagation speed has a limiting value, which corresponds to the planar premixed flame speed; the propagation velocity is slightly higher for the linear case than for the hyperbolic case; increasing the upstream transverse mixture gradient causes a reduction of the triple-flame propagation velocity and an increase of the flame front curvature; the flame front shape is highly asymmetric with respect to the stoichiometric line; the maximum reaction-rate point is located at the fuel-lean side, while the triple flame leading point is located at the fuel-rich side. Both points get closer to the stoichiometric line as the upstream mixture gradient is increased. Using unmatched chemical kinetics with unitary mass fraction exponents results in symmetric flame structures with respect to the stoichiometric line, and maximum reaction rate and most forward points located at the stoichiometric line. Thus, the use of unmatched kinetics leads to solutions that do not represent qualitatively real triple flame structure. However, flammability limit extension and pentasectional character of the triple flame still appear.

Even though the heat release effects have been relaxed, the work presented in this paper shows the importance of using experimental chemical kinetics data. Heat release causes the streamlines ahead of the flame to diverge due to gas expansion, which at the same time causes the mixture gradient to decrease, especially around the stoichiometric line where heat release effects are more pronounced. The mixture gradient strength increases again farther away from the stoichiometric line, where the streamlines become more parallel. These consequences on the mixture gradient along the flame front would cause changes in the solutions for the flame structure if gas expansion due to heat release were considered. However, asymmetries of the flame front associated with the use of experimental kinetics would still be expected.

A suggested further refinement of the present modelling would be to take density variation into consideration together with the use of experimental chemical kinetics data. More accurate chemical kinetics mechanisms (i.e. multiple-step) would also be desirable, as well as considering suitable non-unity Lewis numbers. A study accounting for these new assumptions together with the imposition of a velocity gradient at the inlet would be expected to affect the x-coordinate at which the flame may be stabilised. Simulations performed in such a study would be helpful for the design of combustion chambers.

Funding

The first author appreciates Balsells Fellowship support.

References

[1] J.W. Dold, *Flame propagation in a nonuniform mixture: Analysis of a slowly varying triple flame*, Combust. Flame 76 (1989), pp. 71–88.

[2] J. Buckmaster and M. Matalon, *Anomalous Lewis number effects in tribrachial flames*, Proc. Combust. Inst. 22 (1988), pp. 1527–1535.

[3] S. Ghosal and L. Vervisch, *Theoretical and numerical study of a symmetrical triple flame using the parabolic flame path approximation*, J. Fluid Mech. 415 (2000), pp. 227–260.

[4] H. Phillips, *Flame in a buoyant methane layer*, Symp. (Int.) Combust. 10 (1965), pp. 1277–1283.

[5] S.H. Chung and B.J. Lee, *On the characteristics of laminar lifted flames in a nonpremixed jet*, Combust. Flame 86 (1991), pp. 62–72.

[6] P.N. Kioni, B. Rogg, K.N.C. Bray, and A. Liñán, *Flame spread in laminar mixing layers: The triple flame*, Combust. Flame 95 (1993), pp. 276–290.

[7] B.J. Lee, J.S. Kim, and S.H. Chung, *Effect of dilution of the liftoff of nonpremixed jet flames*, Proc. Combust. Inst. 25 (1994), pp. 1175–1181.

[8] B.J. Lee and S.H. Chung, *Stabilization of lifted tribrachial flames in a laminar nonpremixed jet*, Combust. Flame 109 (1997), pp. 163–172.

[9] T. Plessing, P. Terhoeven, N. Peters, and M.S. Mansour, *An experimental and numerical study of a laminar triple flame*, Combust. Flame 115 (1998), pp. 335–353.

[10] Y.S. Ko, T.M. Chung, and S.H. Chung, *Characteristics of propagating tribrachial flames in counterflow*, KSME Int. J. 16 (2002), pp. 1710–1718.

[11] T.K. Pham, D. Dunn-Rankin, and W.A. Sirignano, *Flame structure in small-scale liquid film combustors*, Proc. Combust. Inst. 31 (2006), pp. 3269–3275.

[12] S.H. Chung, *Stabilization, propagation and instability of tribrachial triple flames*, Proc. Combust. Inst. 31 (2007), pp. 877–892.

[13] J.R. Bellan and W.A. Sirignano, *A theory of turbulent flame development and nitric oxide formation in stratified charge internal combustion engines*, Combust. Sci. Technol. 8 (1973), pp. 51–68.

[14] N. Peters, *Laminar flamelet concepts in turbulent combustion*, Symp. (Int.) Combust. 21 (1988), pp. 1231–1250.

[15] J.W. Dold, L.J. Hartley, and D. Green, *Dynamics of laminar triple-flamelet structures in non-premixed turbulent combustion, in Dynamical Issues in Combustion Theory*, P.C. Fife, A. Liñán, and F. Williams, eds., The IMA Volumes in Mathematics and its Applications Vol. 35, Springer, New York, 1991, pp. 83–105. Available at http://dx.doi.org/10.1007/978-1-4612-0947-8_4.

[16] J.Y. Chen and T. Echekki, *Numerical study of buoyancy effects on triple flames*, Western States Spring Meeting, The Combustion Institute, 13–14 March 2000, Paper number WS 00S-11.

[17] L.J. Hartley and J.W. Dold, *Flame propagation in a nonuniform mixture: Analysis of a propagating triple flame*, Combust. Sci. Technol. 80 (1991), pp. 23–46.

[18] G.R. Ruetsch, L. Vervisch, and A. Liñán, *Effects of heat release on triple flames*, Phys. Fluids 7 (1995), pp. 1447–1454.

[19] P. Domingo and L. Vervisch, *Triple flames and partially premixed combustion in autoignition of non-premixed turbulent mixtures*, Proc. Combust. Inst. 26 (1996), pp. 233–240.

[20] T.G. Vedarajan and J. Buckmaster, *Edge-flames in homogeneous mixtures*, Combust. Flame 114 (1998), pp. 267–273.

[21] J. Daou and A. Liñán, *Triple flames in mixing layers with nonunity Lewis numbers*, Symp. (Int.) Combust. 27 (1998), pp. 667–674.

[22] T. Echekki and J.H. Chen, *Structure and propagation of methanol-air triple flames – physical and chemical fundamentals, modeling and simulation, experiments, pollutant formation*, Combust. Flame 114 (1998), pp. 231–245.

[23] H.G. Im and J.H. Chen, *Structure and propagation of triple flames in partially premixed hydrogen–air mixtures*, Combust. Flame 119 (1999), pp. 436–454.

[24] H.G. Im and J.H. Chen, *Effects of flow strain on triple flame propagation*, Combust. Flame 126 (2001), pp. 1384–1392.

[25] E. Fernández, M. Vera, and A. Liñán, *Liftoff and blowoff of a diffusion flame between parallel streams of fuel and air*, Combust. Flame 144 (2005), pp. 261–276.

[26] C. Jiménez and B. Cuenot, *DNS study of stabilization of turbulent triple flames by hot gases*, Proc. Combust. Inst. 31 (2007), pp. 1649–1656.

[27] C.K. Westbrook and F.L. Dryer, *Chemical kinetic modeling of hydrocarbon combustion*, Prog. Energy Combust. Sci. 10 (1984), pp. 1–57.

[28] J. Buckmaster, *Edge-flames*, Prog. Energy Combust. Sci. 28 (2002), pp. 435–475.
[29] S.R. Turns, *An Introduction to Combustion Concepts and Applications*, 3rd ed., McGraw-Hill Science/Engineering/Math, New York. 2011.
[30] N.D. Sandham and W.C. Reynolds, *Compressible mixing layer: Linear theory and direct simulation*, AIAA J. 28 (1990), pp. 618–624.
[31] M. Zhuang, T. Kubota, and P.E. Dimotakis, *Instability of inviscid, compressible free shear layers*, AIAA J. 28 (1990), pp. 1728–1733.
[32] H. Berestycki, B. Larrouturou, and J. Roquejoffre, *Mathematical investigation of the cold boundary difficulty in flame propagation theory*, in *Dynamical Issues in Combustion Theory*, P.C. Fife, A. Liñán, and F. Williams, eds., The IMA Volumes in Mathematics and its Applications Vol. 35, Springer, New York, 1991, pp. 37–61. Available at http://dx.doi.org/10.1007/978-1-4612-0947-8_2.